High precision optical cavity length and width measurements using double modulation

A. Staley,[1,*] D. Hoak,[2,3] A. Effler,[4] K. Izumi,[5] S. Dwyer,[5] K. Kawabe,[5] E. J. King,[6] M. Rakhmanov,[7] R. L. Savage,[5] and D. Sigg[5]

[1]*Department of Physics, Columbia University, New York, NY 10027, USA*
[2]*University of Massachusetts Amherst, Amherst, MA 01003, USA*
[3] *dhoak@physics.umass.edu*
[4]*LIGO, California Institute of Technology, Pasadena, CA 91125, USA*
[5] *LIGO Hanford Observatory, PO Box 159, Richland, WA 99352, USA*
[6]*University of Adelaide, Adelaide, SA 5005, Australia*
[7]*The University of Texas at Brownsville, Brownsville, TX 78520, USA*

[*] *ans2161@columbia.edu*

Abstract: We use doubly phase modulated light to measure both the length and the linewidth of an optical resonator with high precision. The first modulation is at RF frequencies and is set near a multiple of the free spectral range, whereas the second modulation is at audio frequencies to eliminate offset errors at DC. The light in transmission or in reflection of the optical resonator is demodulated while sweeping the RF frequency over the optical resonance. We derive expressions for the demodulated power in transmission, and show that the zero crossings of the demodulated signal in transmission serve as a precise measure of the cavity linewidth at half maximum intensity. We demonstrate the technique on two resonant cavities, with lengths 16 m and a 4 km, and achieve an absolute length accuracy as low as 70 ppb. The cavity width for the 16 m cavity was determined with an accuracy of approximately 6000 ppm. Through an analysis of the systematic errors we show that this result could be substantially improved with the reduction of technical sources of uncertainty.

OCIS codes: (120.5060) Phase modulation; (140.4780) Optical resonators; (120.3940) Metrology; (120.2230) Fabry-Perot; (040.2840) Heterodyne.

References and links

1. R. Drever, J. Hall, F. Kowalski, J. Hough, G. Ford, A. Munley, and H. Ward, "Laser phase and frequency stabilization using an optical resonator," Appl. Phys. B **31**, 97 (1983).
2. K. D. Skeldon and K. A. Strain, "Response of a Fabry–Perot optical cavity to phase modulation sidebands for use in electro-optic control systems," Appl. Opt. **36**, 6802 (1997).
3. K. D. Skeldon and K. A. Strain, "Response of a Fabry–Perot optical cavity to phase modulation sidebands for use in electro-optic control systems: errata," Appl. Opt. **37**, 4936 (1998).
4. P. J. Manson, "High precision free spectral range measurement using a phase modulated laser beam," Rev. of Sci. Inst. **70**, 3834 (1999).
5. A. Araya, S. Telada, K. Tochikubo, S. Taniguchi, R. Takahashi, K. Kawabe, D. Tatsumi, T. Yamazaki, S. Kawamura, S. Miyoki, S. Moriwaki, M. Musha, S. Nagano, M. K. Fujimoto, K. Horikoshi, N. Mio, Y. Naito,

#241606 Received 26 May 2015; revised 2 Jul 2015; accepted 7 Jul 2015; published 17 Jul 2015

A. Takamori, and K. Yamamoto, "Absolute-length determination of a long-baseline Fabry–Perot cavity by means of resonating modulation sidebands," Appl. Opt. **38**, 2848 (1999).
6. M. Aketagawa, S. Kimura, T. Yashiki, H. Iwata, T. Q. Banh, and K. Hirata, "Measurement of a free spectral range of a Fabry–Perot cavity using frequency modulation and null method under off-resonance conditions," Meas. Sci. and Tech. **22**, 025302 (2011).
7. M. Aketagawa, T. Yashiki, S. Kimura, and T. Banh, "Free spectral range measurement of Fabry–Perot cavity using frequency modulation," Int. Jour. of Precision Engineering and Manufacturing **11**, 851 (2010).
8. B. J. J. Slagmolen, M. B. Gray, K. G. Baigent, and D. E. McClelland, "Phase-sensitive reflection technique for characterization of a Fabry–Perot interferometer," Appl. Opt. **39**, 3638 (2000).
9. M. Rakhmanov, F. Bondu, O. Debieu, and R. L. Savage, "Characterization of the LIGO 4 km Fabry–Perot cavities via their high-frequency dynamic responses to length and frequency variations," Class. Quantum Grav. **21**, S487 (2004).
10. T. Andreae, W. Konig, R. Wynands, D. Leibfried, F. Schmidt-Kaler, C. Zimmermann, D. Meschede, T. W. Hansch, "Absolute frequency measurement of the hydrogen 1S-2S transition and a new value of the Rydberg constant," Phys. Rev. Lett. **69**, 1923-1926 (1992).
11. A. E. Siegman, *Lasers*, (University Science Books, 1986).
12. A. Abramovici, W. E. Althouse, R. W. P. Drever, Y. Gursel, S. Kawamura, F. J. Raab, D. Shoemaker, L. Sievers, R. E. Spero, K. S. Thorne, R. E. Vogt, R. Weiss, S. E. Whitecomb, M. E. Zucker, "LIGO: the Laser Interferometer Gravitational-wave Observatory," Science **256**, 325 (1992).
13. The LIGO Scientific Collaboration, "Advanced LIGO," Class. Quantum Grav. **32**, 074001 (2015).
14. N. C. Wong and J. L. Hall, "Servo control of amplitude modulation in frequency-modulation spectroscopy: demonstration of shot-noise-limited detection," J. Opt. Soc. Am. B **2**, 1527 (1985).
15. E. A. Whittaker, M. Gehrtz, and G. C. Bjorklund, "Residual amplitude modulation in laser electro-optic phase modulation," J. Opt. Soc. Am. B **2**, 1320 (1985).
16. W. Zhang, M. J. Martin, C. Benko, J. L. Hall, J. Ye, C. Hagemann, T. Legero, U. Sterr, F. Riehle, G. D. Cole, and M. Aspelmeyer, "Reduction of residual amplitude modulation to 1×10^{-6} for frequency modulation and laser stabilization," Opt. Lett. **39**, 1980 (2014).
17. R. W. P. Drever, *The Detection of Gravitational Waves*, edited by D. G. Blair (Cambridge University, 1991).
18. A. Staley, D. Martynov, R. Abbott, R. X. Adhikari, K. Arai, S. Ballmer, L. Barsotti, A. F. Brooks, R. T. DeRosa, S. Dwyer, A. Effler, M. Evans, P. Fritschel, V. V. Frolov, C. Gray, C. J. Guido, R. Gustafson, M. Heintze, D. Hoak, K. Izumi, K. Kawabe, E. J. King, J. S. Kissel, K. Kokeyama, M. Landry, D. E. McClelland, J. Miller, A. Mullavey, B. O'Reilly, J. G. Rollins, J. R. Sanders, R. M. S. Schofield, D. Sigg, B. J. J. Slagmolen, N. D. Smith-Lefebvre, G. Vajente, R. L. Ward, and C. Wipf, "Achieving resonance in the Advanced LIGO gravitational-wave interferometer," Class. Quantum Grav. **31**, 245010 (2014).

1. Introduction

A Fabry-Perot cavity near resonance can be used to convert phase modulated laser light into amplitude modulation. If the laser is phase modulated at a single RF frequency using an electro-optic modulator, this effect is proportional to the offset of the carrier frequency from resonance for small deviations. The Pound-Drever-Hall (PDH) technique [1] takes advantage of this to lock the cavity on resonance. However, if the RF sidebands are simultaneously resonant the amplitude modulation vanishes for all frequency offsets. We exploit this property by dithering the laser frequency or cavity length around the resonant point and by sweeping the RF frequency over a resonance near a multiple of the free spectral range. The measured amplitude modulation then shows zero crossings at the multiple of the free spectral range as well as near each half maximum point of the resonance.

The technique was first documented in 1997. A Glasgow group realized that the transmitted RF modulation could be useful to tune the RF frequency such that the sidebands maximally transmit though a mode cleaner [2, 3]. In their method they did not apply a synchronous demodulation, but instead used the amount of the residual amplitude modulation to find the resonant RF frequency.

Further mathematical effort was performed by P. Manson in 1999 [4]. He demonstrated that a small offset in the carrier locking point was necessary to generate the amplitude modulation in transmission. He also performed an experiment and reported that the residual amplitude modulation would strongly affect the precision of estimating the free-spectral range, but gave no

#241606 Received 26 May 2015; revised 2 Jul 2015; accepted 7 Jul 2015; published 17 Jul 2015

quantitative arguments. In parallel, a novel double-demodulation technique was demonstrated by TAMA in 1999 [5] which introduced dithering of the carrier locking point rather than a static offset. The RF sidebands in reflection were locked on a resonance to track the change in the absolute length of a 300 m suspended cavity.

In recent years, the method has been investigated by a Japanese group [6, 7] and an initial analysis of the uncertainties was performed. Despite these efforts, there has been no application of the method for estimating the cavity linewidth. A related approach was used by an ANU group in 2000 [8], in which the phase information in reflection was used to measure the cavity linewidth by determining the turning points in the response. In 2003, another method using frequency modulated light and tuning of the PDH sideband frequency was used at the LIGO Hanford Observatory to measure the 4 km cavity lengths [9].

In this paper, we demonstrate that the amplitude modulation in transmission can be used as a precise measure of the cavity linewidth, and we exploit the double demodulation of an optical resonator to measure the cavity length and linewidth to high precision. We apply the same double-demodulation technique to measure the cavity length using the reflected signal. The technique uses one modulation frequency at RF and the other at audio frequency; the second modulation at audio frequency is important to increase the accuracy of the measurement by avoiding electronics noise at DC. The audio modulation also reduces the coupling of Residual Amplitude Modulation (RAM) to the measurement. We provide the analytic expression to both transmitted and reflected signals, and a detailed analysis of statistical and systematic uncertainties.

With measurements of the cavity length and linewidth, the round-trip reflectivity and finesse can be calculated. In particular, the cavity finesse can be used to deduce the intra-cavity power build up, the average number of photon round trips in the cavity, and the size of the linear range of the Pound-Drever-Hall reflection locking signal. All of this information is vital to locking and characterizing the Advanced LIGO interferometer. In multi-cavity configurations more than one set of RF modulation sidebands are generally needed for locking. Typically, at least one RF wavelength will be set to a multiple of one of the cavity lengths—requiring an accurate length measurement. Precise measurements of the cavity linewidth is a useful tool to characterize the transmission coefficients and losses of the cavity mirrors. Furthermore, long term monitoring gives insights into mirror degradation due to contamination.

The usefulness of these measurements can be extended outside of Advanced LIGO. As highlighted in Ref. [7], length measurements with small uncertainty are required in the field of nanotechnology and ultra precision engineering. Fabry-Perot interferometers are also used for spectroscopy [10] and laser calibration [11]. Characterization of Fabry-Perot interferometers to high precision has important applications in optical metrology such as mirror characterization and contamination studies.

This paper is organized as follows. The experimental setup is described in Section 2 and the equations for the transmitted signal are presented in Section 3. Section 4 assess the accuracy of the technique for various sources of statistical and systematic error. In Section 5 we present the results obtained from applying this measurement on two different-length suspended cavities of the Laser Interferometer Gravitational-wave Observatory (LIGO) [12, 13], where this technique was first used in 2004. We conclude with a summary of the limiting sources of uncertainty for the technique.

#241606 Received 26 May 2015; revised 2 Jul 2015; accepted 7 Jul 2015; published 17 Jul 2015

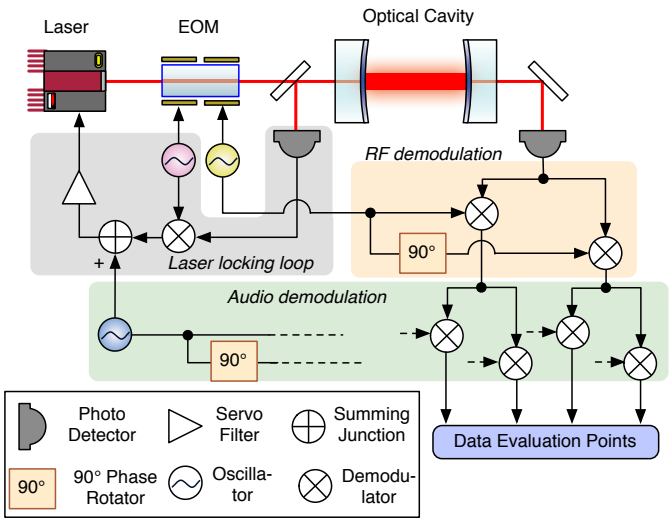

Fig. 1. Measurement setup. A laser beam is doubly phase modulated using an electro-optic modulator (EOM) and then locked to an optical cavity. The first phase modulation is used for deriving a cavity length signal using the Pound-Drever-Hall reflection locking technique. The second phase modulation is used to generate RF sidebands near a multiple of the full spectral range.

2. Setup

The measurement setup is shown in Fig. 1. The light of a laser source is modulated by an electro-optic modulator (EOM) at two RF frequencies. The first frequency, at a large offset from the cavity resonance, is used with a photodetector in reflection for locking the cavity with the Pound-Drever-Hall technique. This servo feeds back to the laser to keep its frequency locked on the cavity resonance. The second RF frequency, f_{RF}, is used for generating RF sidebands near a multiple of the free spectral range. This frequency is then swept over the cavity linewidth during the measurement. A third frequency in the audio band, f_a, is used to slightly detune the laser from the cavity resonance by adding a small electronic offset to the laser locking loop. A photodetector in transmission (or reflection) of the cavity is used to complete the measurement. Its output is first demodulated at f_{RF} to form an in-phase and a quadrature-phase down-converted output. The two outputs are acquired by analog-to-digital converters, and digitally demodulated a second time at the audio frequency f_a.

3. Theory

The RF modulation is applied at frequency f_{RF} with a phase modulation index Γ. The phase of the laser light can then be written as $\varphi(t) = \Gamma \cos 2\pi f_{\mathrm{RF}} t$. A second modulation at audio frequency f_a is applied to the laser frequency with strength δf, i.e., $f(t) = f_0 + \delta f \cos 2\pi f_a t$, where f_0 is the laser carrier frequency. For our measurements we operate in the phase modulation regime and require that $\delta f \ll f_a$. The double demodulated signal in transmission of the cavity can then be written as:

#241606 Received 26 May 2015; revised 2 Jul 2015; accepted 7 Jul 2015; published 17 Jul 2015

$$S_{tr}(\phi_f,\phi_a) = S_{tr}(\phi_f)\frac{(1-R)\left(e^{i\phi_f}-R\right)}{\left(e^{i\phi_f+i\phi_a}-R\right)\left(e^{i\phi_f}-e^{i\phi_a}R\right)(1-2R\cos\phi_a+R^2)} \times \begin{cases} \dfrac{e^{2i\phi_a}-1}{2i\phi_a}\left(e^{i\phi_f}(1-R)-R(1-2R\cos\phi_a+R)\right) & \text{audio in-phase} \\ \dfrac{\left(e^{i\phi_a}-1\right)^2}{2\phi_a}\left(e^{i\phi_f}(1+R)+R(1-2R\cos\phi_a-R)\right) & \text{audio quad-phase} \end{cases} \quad (1)$$

$$S_{tr}(\phi_f) = p_0\, g_{tr}^2\, R\, e^{i\phi_f}\frac{1-e^{i\phi_f}}{(e^{i\phi_f}-R)^2} = p_0\, g_{tr}^2\,\frac{-2R}{\left(1-2R\cos\phi_f+R^2\right)^2}\sin\frac{\phi_f}{2} \times\left[\sin\frac{\phi_f}{2}\left(1+2R-(1+2\cos\phi_f)R^2\right)+i\cos\frac{\phi_f}{2}\left(1-2R-(1-2\cos\phi_f)R^2\right)\right] \quad (2)$$

$$\text{with}\;\; p_0 = 2\pi\frac{\delta f}{f_{\mathrm{FSR}}}\Gamma P_{\mathrm{in}},\;\; g_{tr}^2 = \frac{(1-r_1^2)(1-r_2^2)}{(1-R)^2},\;\; R = r_1 r_2,\;\; f_{\mathrm{FSR}} = \frac{c}{2L},$$

$$\phi_a = 2\pi\frac{f_{\mathrm{a}}}{f_{\mathrm{FSR}}}\;\;\text{and}\;\;\phi_f = 2\pi\frac{f_{\mathrm{RF}}}{f_{\mathrm{FSR}}}.$$

The real part describes the RF in-phase signal and the imaginary part the RF quadrature-phase signal. The cavity length is L, P_{in} is the input laser power, and r_1 and r_2 are the amplitude reflectivity coefficients of the input and output mirrors, respectively. If the frequency of the audio modulation is small compared to the cavity linewidth, we can show that

$$\lim_{\phi_a\to 0} S_{tr}^{\mathrm{I}}(\phi_f,\phi_a) = S_{tr}(\phi_f)\;\;\text{and}\;\;\lim_{\phi_a\to 0} S_{tr}^{\mathrm{Q}}(\phi_f,\phi_a) = 0$$

for the in-phase and quadrature-phase terms, respectively. The theoretical signal for a cavity with $R = 0.98$ and $\phi_a \to 0$ is shown in Fig. 2.

Realistic mirrors have $0 < R < 1$ which leads to $1+2R-(1+2\cos\phi_f)R^2 > 0$ for all ϕ_f. Hence, the in-phase signal is strictly negative with the exception of zeros at $f_0 = nf_{\mathrm{FSR}}$ due to the sine term. This is the only true zero of the doubly demodulated signal S_{tr}. The quadrature-phase signal has additional zeroes: one is located at $f_1 = (n+\frac{1}{2})f_{\mathrm{FSR}}$ and is not interesting. Setting $1-2R-(1-2\cos\phi_f)R^2 = 0$, we find two additional zeros at

$$f_{\pm} = \pm\frac{f_{\mathrm{FSR}}}{\pi}\sin^{-1}\left(\frac{\pi}{2\mathscr{F}\sqrt{R}}\right)+nf_{\mathrm{FSR}} = \pm\frac{f_{\mathrm{pole}}}{\sqrt{R}}+nf_{\mathrm{FSR}}$$
$$\text{with}\;\; f_{\mathrm{pole}} \approx \frac{f_{\mathrm{FSR}}}{2\mathscr{F}}\;\;\text{and}\;\;\mathscr{F} = \frac{\pi\sqrt{R}}{1-R}. \quad (3)$$

where we use $\mathscr{F}$ to denote the finesse of the optical cavity, and where f_{FSR} denotes the free-spectral-range of the cavity. We can see that the difference between the two secondary zero crossing is equal to the cavity linewidth divided by $\sqrt{R}$.

4. Analysis and uncertainties

The FSR can be measured to high precision from the main zero crossing; the measured frequency is simply divided by the order n. The cavity length can then be calculated accordingly.

The two secondary zero crossings of the quadrature-phase signal provide important information about the optical cavity. In particular, the expression for $f_{\pm}$ depends only on the FSR of the cavity and on the round-trip reflectivity R. Thus the measurement of the secondary zero

#241606 Received 26 May 2015; revised 2 Jul 2015; accepted 7 Jul 2015; published 17 Jul 2015

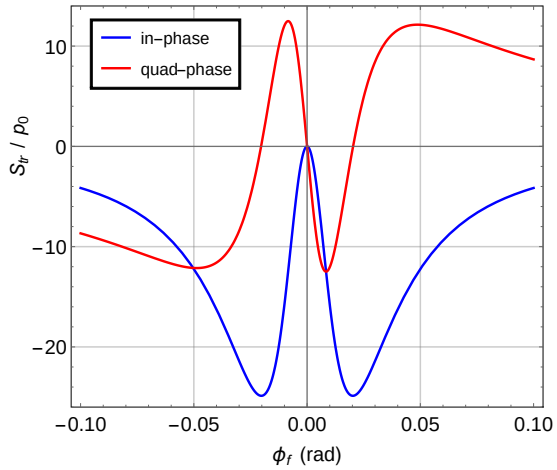

Fig. 2. Double demodulation signal in transmission of a cavity with $\phi_a \to 0$. Shown are the RF in-phase and quadrature-phase signals assuming the audio modulation frequency is small compared to the cavity linewidth. The finesse of the cavity is $\mathscr{F} = 156$. The exact position of the secondary zero crossings also depends on the time delay between the optical path and the RF demodulation path. The signals are shown for zero delay.

crossings can be inverted using Eq. (3) to obtain a precise measure of the round-trip reflectivity R. This is then used to calculate the cavity finesse and the cavity pole frequency (halfwidth), $f_{\rm pole}$, which characterizes the dynamical response of the laser field on resonance.

The remainder of this section provides a comprehensive discussion of the measurement uncertainties.

4.1. Timing accuracy

Any systematic offset in the measurement of the RF frequency will directly translate into length errors. The measurement of the cavity linewidth will be immune to static offsets, but a changing relative frequency error will shift the secondary zero crossings. GPS synchronization can be used to stabilize an RF frequency source to the ppb level. For the experimental demonstration, we used a GPS synchronized RF source and verified its accuracy with a frequency counter which was also synchronized to GPS. An accuracy of $< 10^{-7}$ and $< 10^{-8}$ was achieved over $T = 1\,\mathrm{s}$ and $T = 10\,\mathrm{s}$ measurement periods, respectively.

4.2. Sensing noise

Sensing noise will typically be composed of shot noise and electronics noise. Any fixed electronics offsets will be rejected by the use of the audio modulation. For simplicity, we assume that the transmission and reflection photodetectors are shot noise limited. At each free spectral range the transmitted power will be $g_{tr}^2 P_{\rm in}$. The shot noise is then given by $\sqrt{2 g_{tr}^2 P_{\rm in} hc/\lambda}$, with λ the laser wavelength.

To calculate the effect of uncertainty from shot noise on the zero crossings, we evaluate the derivatives of Eq. (2) at the zero crossings:

$$\left.\frac{d\,S_{tr}}{d\phi_f}\right|_{\phi_f=0} = -p_0\, g_{tr}^2\, \frac{R}{(1-R)^2} \approx -\frac{2}{R}\left.\frac{d\,S_{tr}}{d\phi_f}\right|_{\phi_f=\phi_\pm}$$

#241606 Received 26 May 2015; revised 2 Jul 2015; accepted 7 Jul 2015; published 17 Jul 2015

The frequency error due to shot noise can then be written as

$$\Delta f_{\mathrm{RF}}^{\mathrm{shot}} = \frac{(1-R)^2}{R}\sqrt{\frac{2hc}{\lambda\, g_{lr}^2 P_{\mathrm{in}} T}}\left(\frac{1}{\delta f\,\Gamma}\right)\left(\frac{f_{\mathrm{FSR}}}{2\pi}\right)^2 \tag{4}$$

with T the measurement period. At the half maximum points a similar equation can be derived. Since the power at the secondary zero crossings is only half and the slope is roughly half, the frequency error becomes approximately $\sqrt{2}$ smaller.

4.3. Audio modulation frequency response

When deriving Eq. (2), we assumed that the audio modulation frequency is small compared to the cavity linewidth. Relaxing this condition will generate a phase shift in the corresponding demodulated signal. This will not affect the cavity length measurement, but it will increase the separation of the zeroes near the half maximum points. The zero crossing of the in-phase audio modulation component can be approximated by

$$f_{\pm}(\phi_a) = f_{\pm}\left(1+\frac{\phi_a^2}{R f_{\pm}^2}\right).$$

For $R > 0.8$ and $\phi_a < 0.1 f_{\pm}$ the approximation is better than 150 ppm; and 1 ppm or less for $\phi_a < 0.01 f_{\pm}$. The exact equation can be used for higher audio frequencies, or when higher accuracy is required.

4.4. RF modulation phase variations

RF phase shifts do not affect the zero crossing at the free spectral range, because both in-phase and quadrature-phase terms are simultaneously zero. However, at the half maximum points, the in-phase signal is near maximum and will admix into the quadrature-phase with a demodulation phase error. We distinguish between common and differential RF phase shifts. To first order a common RF phase error will shift the secondary zero crossings in the same direction. Hence, if we calculate the linewidth by taking the difference between the two secondary zero crossings, we are first order insensitive to small common RF phase errors. Differential RF phase errors will directly change the linewidth measurement.

A time delay will produce a common RF phase shift at a fixed frequency. But due to its linear frequency dependency, it will also produce a differential RF phase shift. The latter needs to be taken into account, if the delay is significant relative to the RF signal period. This is certainly true in our case, since the cavity geometry is of the same scale as the RF wavelength. The electro-optic modulator and the RF demodulation electronics can also generate a differential phase shift—especially if they include tuned resonant circuits. Again, this is not a problem for the length determination, but it can easily be the dominant uncertainty in the linewidth measurement. We write the frequency error due to a differential RF phase variation $\Delta\phi_{\mathrm{RF}}$ between the half maximum points as

$$\Delta f_{\mathrm{RF}}^{\mathrm{phase}} \approx (1-R)\,\Delta\phi_{\mathrm{RF}}\frac{f_{\mathrm{FSR}}}{2\pi} \approx \Delta\phi_{\mathrm{RF}} f_{\mathrm{pole}}. \tag{5}$$

4.5. Cavity length fluctuations

Due to the double demodulation scheme this technique is first order insensitive to any electronics offset, such as offsets in the locking servo amplifier, as well as locking point offsets in the cavity. Length measurements utilizing only a single modulation frequency are not immune to DC offsets in the signal chain, which introduce an error. The addition of the audio frequency

#241606 Received 26 May 2015; revised 2 Jul 2015; accepted 7 Jul 2015; published 17 Jul 2015

modulation behaves as a second lock-in amplifier and nulls this uncertainty. However, both cavity length and laser frequency variations at the audio frequency will appear as statistical uncertainties in the measurement. They can always be minimized by increasing the measurement time.

4.6. Higher order RF modulation terms

Aketagawa et al [6] derive an expression for the reflected and transmitted signal with a single RF demodulation including higher-order RF modes. Including higher-order RF terms in Eq. (2) increases the slope of the quadrature-phase signal at the main zero crossing, and shifts the location of the secondary zero crossings inward. Thus the effect of the higher-order RF terms is to improve the accuracy of the length measurement, but to bias the measurement of the linewidth. The bias is proportional to Γ^2, the square of the RF modulation index.

4.7. Residual amplitude modulation noise (RAM)

RAM is a significant problem for high precision cavity locking using the Pound-Drever-Hall technique. RAM generated in the electro-optic modulator has been characterized [14, 15] and active suppression schemes have been developed [16]. The technique presented here is intrinsically less sensitive to RAM because of the double demodulation.

We can model the effect of RAM at both RF and audio frequencies as a modulation of the input field to the cavity. If we multiply the input field by the following term,

$$\left(1+\varepsilon\Gamma\cos(2\pi f_{\mathrm{RF}}t-\psi)\right)\left(1+\eta\,\frac{\delta f}{2\pi f_a}\sin 2\pi f_a t\right),$$

we get a signal in transmission with terms bilinear in the coefficients ε and η:

$$S_{tr}^{\mathrm{AM}}(\phi_f) = -p_0\, g_{tr}^2\, R\, e^{i\phi_f}\,\frac{1+e^{i\phi_f}-2R}{(e^{i\phi_f}-R)^2}\,e^{i\psi}\varepsilon\eta. \tag{6}$$

The coefficients ε and η describe the fraction of amplitude modulation relative to the RF and audio phase modulation, respectively. Neither a RAM generated by the electro-optic modulator nor the laser has an effect on its own. Furthermore, the RAM generated by the audio modulation of the laser frequency and therefore η can always be suppressed with an intensity stabilization servo system. For the length measurement the signal due to the RAM becomes:

$$S_{tr}^{\mathrm{AM}}(0) = p_0\, g_{tr}^2\,\frac{2R}{1-R}\,e^{i\psi}\varepsilon\eta. \tag{7}$$

One can see that the quadrature phase signal is only sensitive to the RF RAM generated in the quadrature-phase. The above equations do not include a RAM generated in the quadrature phase of the frequency modulation. This term will always appear in the quadrature phase of the audio demodulation, but is not important for small audio frequencies.

5. Results

We applied the double-demodulation technique to two of the optical cavities in the advanced LIGO Hanford detector. The cavities are the 16 m input mode cleaner, a triangular cavity that suppresses higher order mode content on the input beam and stabilizes the laser frequency, and one of the 4 km Fabry-Perot arm cavities [17, 13].

#241606 Received 26 May 2015; revised 2 Jul 2015; accepted 7 Jul 2015; published 17 Jul 2015

5.1. 16 m cavity

For the input mode cleaner, we used two RF modulation frequencies, one around the free spectral range of 9.1 MHz and a second at five times the free spectral range near 45.5 MHz. We applied three different audio frequency modulations, at 103 Hz, 303 Hz, and 1 kHz. The variety of RF and audio modulation frequencies was used to check our sensitivity to particular elements of the readout chain and to estimate some of our systematic uncertainties.

The setup is as described in Section 2, where the light source is the main 1064 nm laser of the interferometer, and the photodetector for the double-demodulation is in transmission. The RF frequency was scanned across a range slightly larger than the cavity linewidth. In our setup the audio frequency was not negligible compared to the cavity linewidth. It also included an unknown optical delay. Since both of these parameters have a small effect on the position of the secondary zero crossings, we account for this by fitting Eq. (1) to the data using a seven-parameter nonlinear least-squares fit. The seven parameters included an overall amplitude coefficient, A, the free spectral range of the cavity, f_{FSR}, and the round-trip reflectivity of the mirrors, R. Two other parameters, f_{EOM} and Q, were used to characterize the response of the resonant circuit in the EOM used to generate the RF sidebands. The effect of this circuit was to change the phase and amplitude response of the system as a function of frequency; the fit treated the circuit response as a Lorentzian function with central frequency, f_{EOM}, and width, f_{EOM}/Q. The fit results for these parameters were in good agreement with independent measurements of the EOM response. Finally, two additional parameters, θ_0 and ϕ_0, were used to account for static phase delays between the modulation and demodulation of the RF and audio sidebands, respectively. Overall, the seven fit parameters were found to be consistent across the six data sets consisting of two RF frequencies with three audio frequencies each.

Table 1. Results from the fit of Eq. (1) to the data of the 16 m input mode cleaner cavity.

Parameter	Fit result	Stat. Uncertainty
f_{FSR} (Hz)	9100235.6	$\pm$2.8
R	0.9939317	$\pm$0.0000026

Data for the 1 kHz modulation for the input mode cleaner is presented in Fig. 3, along with fit lines and residuals. We estimate our 67% confidence level uncertainties using the statistical errors derived from the nonlinear fit to the data, as well as the variation in the fit parameters across data sets and across permutations of data selection and downsampling. The results of the fit for the important physical parameters along with their 67% statistical uncertainties are presented in Table 1. Following Eq. (3), the cavity length and linewidth are calculated using the measured FSR and round-trip reflectivity. For each of these parameters, results from the six data sets are combined using a straight-forward χ^2 estimation. These final results are given in Table 2 along with their statistical uncertainty.

5.2. 4 km cavity

The length of a single 4 km arm cavity was also measured with the double-demodulation technique, albeit with some slight modifications in the setup. Instead of using the interferometer's main infrared beam as the light source, as used for the input mode cleaner measurement, we used an auxiliary green laser that is nominally used to lock the arm cavities separately [18]. Additionally, the double-demodulation signal was measured in reflection, instead of in transmission. The expression for the signal in reflection can be found in Appendix B.

As before, we applied the three audio modulation frequencies at 103 Hz, 303 Hz, and 1 kHz.

#241606 Received 26 May 2015; revised 2 Jul 2015; accepted 7 Jul 2015; published 17 Jul 2015

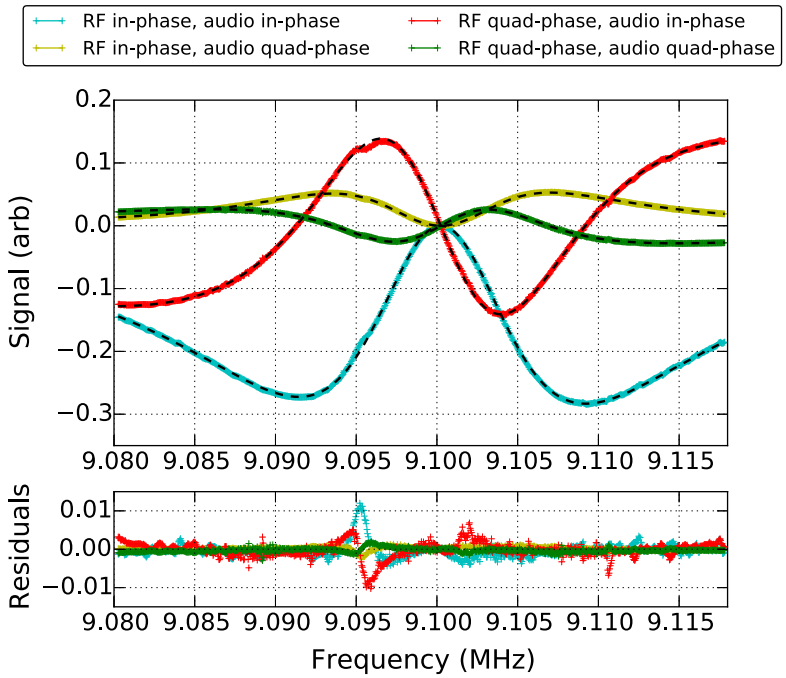

Fig. 3. The black dashed traces represent the fit of Eq. (1) to the double-demodulated data for a 16 m cavity. For this data, the audio modulation frequency was 1 kHz, and the RF modulation frequency was scanned from 9.08 to 9.12 MHz. The deviation from the model around 9.095 MHz is due to an unknown feature in the signal path. Masking out the data in a 5 kHz band around this feature does not change the results of the parameter estimation.

Applying a linear fit to the quadrature-phase signal near the main zero crossing, the length of the cavity was measured to sub-millimeter precision. The cavity pole was not measured, since the linewidth is around 2.9 kHz and of little relevance. The results are listed in Table 2.

Table 2. The top rows show the derived length and cavity pole from the fit for the 16 m cavity. The bottom rows show the free spectral range and exact length for the 4 km cavity, here $N = 666$. The statistical uncertainties from fitting the data are presented. The systematic errors are discussed is Section 5.3.

Cavity	Parameter	Result	Stat. Uncertainty
16 m	f_{pole} (Hz)	8806	± 10
	L (m)	16.471701	± 0.000003
4 km	$N \times f_{\mathrm{FSR}}$ (Hz)	24992279	± 1
	L (m)	3994.4692	± 0.0002

For the 4 km cavity, our accuracy was limited by reduced finesse due to a manufacturing error in the reflectivity of the input mirror. However, we used an RF modulation frequency of 24.9 MHz, or approximately 666 times the free spectral range of the arm cavity; this in turn greatly enhanced our accuracy. Overall, the relative accuracy of the 4 km cavity length measurement was approximately a factor of four better than the measurement of the 16 m cavity.

#241606 Received 26 May 2015; revised 2 Jul 2015; accepted 7 Jul 2015; published 17 Jul 2015

5.3. *Uncertainties*

In this section we provide details of the estimation of our systematic uncertainties which were discussed in Section 4. Sensor noise such as shot noise is already included in the uncertainties derived from the fit, since it has a statistical behavior. It is also rather small and contributing only at the level of ± 0.01 Hz or less to each measurement point. Since we fit the complete expression given by Eq. (1), we do not account for the approximation of the audio modulation frequency response. The laser locking loop which controlled the laser frequency had high gain, and the residual cavity length fluctuations were too small to be of importance. We are left with the systematic uncertainties due to the accuracy of the frequency determination, variations of the RF modulation phase, the residual amplitude modulation, and the influence of higher order harmonics in the RF modulation. For each of these uncertainties, we calculate quantitative values using the expressions derived in Section 4. The results are summarized in Table 3, expressed as frequency shifts to the relevant zero crossings of the doubly-demodulated signal.

Table 3. Estimated systematic errors in Hertz to the measured frequencies of the main zero crossing (length) and difference between the secondary zero crossings divided by two (used for the cavity pole). The frequency errors are split among the length and linewidth measurements for the 16 m cavity; the linewidth was not measured for the 4 km cavity. These systematic uncertainties are estimated with a 67% confidence level.

Sys. Uncertainty (Hz)	16 m Cavity		4 km Cavity
	Length	f_{pole}	Length
Absolute Timing	1	0	1
RAM	$\ll 0.001$	$\ll 0.001$	$\ll 0.001$
RF Modulation Phase	0	48	0
RF Harmonics	0	4	0
Total	± 1	± 52	± 1

At the time of the measurement the frequency counter was calibrated to ± 1 Hz absolute. This directly translates into a systematic uncertainty in determining the frequency of the main zero crossing. With our RF frequencies of 9.1 MHz, 45.5 MHz and 24.9 MHz this corresponds to a relative error of 100 ppb, 20 ppb and 40 ppb, respectively. The timing error for the width measurement is negligible, since we are computing the difference between the two secondary zero crossings.

The frequency error from the RAM, $S_{tr}^{RAM}(0)$, can be approximated by $\Delta f^{\text{RAM}} \approx \eta \varepsilon f_{\text{pole}} \sin\psi$. Assuming the worst case scenario, with all the RAM in the quadrature phase, we set $\psi = \pi/2$. We measured $\varepsilon \lesssim 10^{-3}$ for the RF modulation and $\eta \lesssim 10^{-5}$ for the audio frequency modulation. The frequency error due to RAM for the width measurement is significantly smaller still. The audio modulation and the small value of η is crucial to make the effect of the RAM insignificant in our measurement.

With these systematic uncertainties, the results for the lengths of the two cavities are:

$$L = 16.471701\,\text{m} \pm 3\mu\text{m}\,(\text{stat}) \pm 1\mu\text{m}\,(\text{sys})$$

and

$$L = 3994.4692\,\text{m} \pm 0.2\text{mm}\,(\text{stat}) \pm 0.2\text{mm}\,(\text{sys}).$$

The model for our fit to the 16 m cavity includes a resonance to account for the tuned circuit of the EOM used to generated the RF sidebands. To investigate our systematics we also used

#241606 Received 26 May 2015; revised 2 Jul 2015; accepted 7 Jul 2015; published 17 Jul 2015

models with linear RF phase and different amplitude terms. The amplitude terms were linear, quadratic, and linear with quadratic. The resulting measurements of $f_{\rm pole}$ varied over a total range of about 100 Hz. For our final result of the cavity pole measurement we take the average and include the standard deviation as a systematic error; in this way we account for the uncertainty of the RF modulation phase.

The higher order RF modulation terms will improve the length measurement, but worsen the linewidth [6]. The modulation depth for the 9.1 MHz and 45.5 MHz modulation frequencies was $\Gamma = 0.20$ and $\Gamma = 0.28$, respectively. Following Appendix A and B, and comparing to Eqs. (9) and (10) of [6], one can extrapolate to the higher-order mode equation for the double-demodulation. Terms of the form $S_{tr}(\phi_f) + \frac{\Gamma^2}{8} S_{tr}(2\phi_f)$ appear in the expression. The secondary zero-crossings used to determine the cavity pole are shifted with the presence of higher order RF modulation terms. Using numerical methods we find a reduction by 42 Hz and 82 Hz of the linewidth for the two modulation frequencies, respectively. Assuming a 10% uncertainty in the modulation depth the uncertainty of this correction to the cavity pole frequency is no larger than 4 Hz.

Including the uncertainty arising from the RF modulation phase and the correction from the RF harmonics, the final result for the cavity pole becomes:

$$f_{\rm pole} = 8804\,{\rm Hz} \pm 10\,{\rm Hz}\ ({\rm stat}) \pm 52\,{\rm Hz}\ ({\rm sys}).$$

6. Conclusions

We have presented a precision measurement technique for the characterization of resonant optical cavities. We have demonstrated this technique on two cavities of the LIGO Hanford gravitational-wave detector, and measured the cavity length to a precision as low as 70 ppb and the width to approximately 6000 ppm.

Our length measurement for the 16 m cavity can probably only be improved by using a substantially higher modulation frequency. At 500 MHz one should be able to achieve sub micron precision. Our measurement of the 4 km cavity length was substantially limited by the poor signal-to-noise due to low finesse. Fixing the coating error will improve the signal in reflection by at least two orders of magnitude (see Appendix B). There is no fundamental limit which would prevent us from improving our timing accuracy by the same amount. This could potentially lead to a cavity length determination below the 1 ppb level. This is well below the length changes introduced by tidal forces which are of order 200 μm and even below the $\sim$5 μm motion of the free swinging test masses.

For our width measurement the largest error is due to the use of a tuned EOM. By using an EOM with flat frequency response and by reducing the modulation depth one could reduce the systematic error below the statistical one, and achieve an accuracy better than 1000 ppm.

A. Audio frequency expansion

In this Appendix we provide details of the derivation of Eq. (1). We begin with a simplified scenario without the audio modulation. Instead, we shift the laser frequency away from resonance by a small fixed offset, δf. We write the laser frequency as $f_0 = N f_{\rm FSR} + \delta f$. Recall, the transmitted electric field is given by,

$$E_t = t(\phi) E_{inc}$$

where the transmission coefficient is defined below and can be expressed in our notation:

$$t(\phi) = \frac{t_1 t_2}{1 - r_1 r_2 e^{i\phi}} = \frac{g_t (1-R)}{1 - R e^{i\phi}}. \tag{8}$$

#241606 Received 26 May 2015; revised 2 Jul 2015; accepted 7 Jul 2015; published 17 Jul 2015

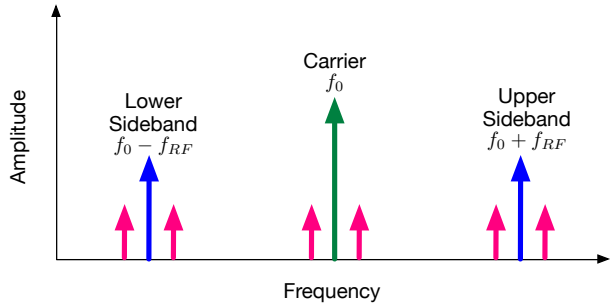

Fig. 4. The green arrow represents the laser frequency, which has an offset δf from the locking point. The RF sidebands produced by the first phase modulation are depicted by the blue arrows. An additional modulation at audio frequencies f_a produces four audio sidebands as seen by the pink arrows. In this case $\delta f \ll f_a$. The plotted amplitudes are arbitrary and depend on the modulation depths.

If we then apply a phase modulation at an RF frequency, f_{RF}, the incident electric field is expressed as

$$E_{inc} = E_0 e^{iN\omega_{\mathrm{FSR}}t} e^{i\delta\omega t} e^{i\Gamma\cos\omega_{\mathrm{RF}}t}.$$

where we switched to a more concise notation using $\omega = 2\pi f$.

Using the Jacobi-Anger expression, the transmitted electric field, expressed in terms of Bessel functions of the first kind, is then

$$E_t = E_0 e^{i\omega_0 t}\left\{J_0(\Gamma)t(\phi_c) + iJ_1(\Gamma)t(\phi_{up}^{sb})e^{i\omega_{\mathrm{RF}}t} + iJ_1(\Gamma)t(\phi_{low}^{sb})e^{-i\omega_{\mathrm{RF}}t}\right\}$$

where

$$\begin{aligned}\phi_c &= \frac{\delta\omega}{f_{\mathrm{FSR}}}\\ \phi_{\mathrm{up,low}}^{\mathrm{sb}} &= \frac{\pm\omega_{\mathrm{RF}} + \delta\omega}{f_{\mathrm{FSR}}} = \pm\phi_f + \phi_c.\end{aligned} \tag{9}$$

The transmitted signal is mixed with a local oscillator of the same RF frequency, and low passed, so that we can extract the terms in the power that oscillate with f_{RF}. The demodulated signal at the photodetector is then given by,

$$\begin{aligned}P_t^{\mathrm{RF}} = 2J_0(\Gamma)J_1(\Gamma)P_{\mathrm{in}}\times & \\ \left\{\mathrm{Im}\left[t(\phi_c)t^*(\phi_{\mathrm{low}}^{\mathrm{sb}}) - t^*(\phi_c)t(\phi_{\mathrm{up}}^{\mathrm{sb}})\right]\cos(\omega_{\mathrm{RF}}t)\right. & \\ \left.+\mathrm{Re}\left[t(\phi_c)t^*(\phi_{\mathrm{low}}^{\mathrm{sb}}) - t^*(\phi_c)t(\phi_{\mathrm{up}}^{\mathrm{sb}})\right]\sin(\omega_{\mathrm{RF}}t)\right\} &\end{aligned} \tag{10}$$

where the cosine term corresponds to the in-phase signal and the sine term is the quadrature phase signal. Notice, that without the frequency offset δf, Eq. (10) is zero. Using Eqs. (8) and (9), along with the following approximations,

$$J_0(\Gamma) \approx 1, \qquad J_1(\Gamma) \approx \Gamma/2, \qquad e^{i\phi_c} \approx 1 + i\phi_c$$

one arrives at Eq. (2).

#241606 Received 26 May 2015; revised 2 Jul 2015; accepted 7 Jul 2015; published 17 Jul 2015

To get the full expression in Eq. (1), a similar derivation is done including the second modulation at the audio frequency, $f_{\rm a}$. The incident electric field becomes,

$$E_{inc} = E_0 e^{iN\omega_{\rm FSR}t} e^{i\delta\omega/\omega_{\rm a}\sin\omega_{\rm a}t} e^{i\Gamma\cos\omega_{\rm RF}t}.$$

The transmitted electric field is now,

$$E_t = E_0 e^{i\omega_0 t} \times \left[J_0(\Gamma)F(\phi_c) + iJ_1(\Gamma)F(\phi_{\rm low}^{\rm sb})e^{-i\omega_{\rm RF}t} + iJ_1(\Gamma)F(\phi_{\rm up}^{\rm sb})e^{i\omega_{\rm RF}t}\right],$$
$$F(\phi) = J_0(\delta\omega/\omega_{\rm a})t(\phi) + J_1(\delta\omega/\omega_{\rm a})t(\phi+\phi_{\rm a})e^{i\omega_{\rm a}t} - J_1(\delta\omega/\omega_{\rm a})t(\phi-\phi_{\rm a})e^{-i\omega_{\rm a}t}$$

such that it describes the carrier field and all the modulated sidebands as depicted in Fig 4. The derivation to Eq. (1) follows as before.

B. Signals in reflection

The equation in reflection follows a similar derivation, with the transmission coefficient $t(\theta)$ replaced everywhere with the reflection coefficient:

$$r(\theta) = -r_1 + \frac{t_1^2 r_2 e^{-i\phi}}{1 - r_1 r_2 e^{-i\phi}} \tag{11}$$

The signal in reflection of the cavity can be written as

$$S_{\rm refl}(\phi_f,\phi_a) = S_{\rm refl}(\phi_f)\frac{e^{i\phi_a}(1-R)\left(e^{i\phi_f}-R\right)}{\left(e^{i\phi_f+i\phi_a}-R\right)\left(e^{i\phi_f}-Re^{i\phi_a}\right)(1-2R\cos\phi_a+R^2)\left(e^{i\phi_f}-r_2^2\right)} \tag{12}$$
$$\times\begin{cases}\times\dfrac{\sin\phi_a}{\phi_a}\left[\left(e^{2i\phi_f}+Rr_2^2\right)(1-R)-e^{i\phi_f}\left((1+R)\left(R-r_2^2\right)-2\cos\phi_a\left(R^2-r_2^2\right)\right)\right]\\ \dfrac{(\cos\phi_a-1)}{\phi_a}\left[\left(e^{2i\phi_f}+Rr_2^2\right)(1+R)+e^{i\phi_f}\left((1-R)\left(R-r_2^2\right)-2\cos\phi_a\left(R^2+r_2^2\right)\right)\right]\end{cases}$$

$$S_{\rm refl}(\phi_f) = p_0\, g_{\rm refl}^2\, R\,\frac{\left(1-e^{i\phi_f}\right)\left(r_2^2-e^{i\phi_f}\right)}{(e^{i\phi_f}-R)^2} = p_0\, g_{\rm refl}^2\,\frac{-2R}{\left(1-2R\cos\phi_f+R^2\right)^2}\sin\frac{\phi_f}{2}$$
$$\times\left[\sin\frac{\phi_f}{2}\left(1+2R-(1+2\cos\phi_f)\left(R^2+r_2^2\right)+Rr_2^2(2+R)\right)\right.$$
$$\left.+\,i\cos\frac{\phi_f}{2}\left(1-2R-(1-2\cos\phi_f)\left(R^2-r_2^2\right)+Rr_2^2(2-R)\right)\right] \tag{13}$$

with $g_{\rm refl}^2 = -\frac{1-r_1^2}{(1-R)^2}$, the first case of Eq. (12) is the audio in-phase, and the second case is the audio quad-phase. If the frequency of the audio modulation is small compared to the cavity linewidth, we can show that

$$\lim_{\phi_a\to 0} S_{\rm refl}^{\rm I}(\phi_f,\phi_a) = S_{\rm refl}(\phi_f)$$
$$\text{and}\quad \lim_{\phi_a\to 0} S_{\rm refl}^{\rm Q}(\phi_f,\phi_a) = 0.$$

for the in-phase and quadrature-phase terms, respectively. The theoretical signals for two cavities with $R = 0.98$ and $\phi_a \to 0$ are shown in Fig. 5. One of the cavities has equal transmission mirrors, whereas the other has a high reflector as the rear mirror. In the first case, the only interesting zeroes are at the origin, and there are no secondary zero crossing near the cavity pole.

#241606 Received 26 May 2015; revised 2 Jul 2015; accepted 7 Jul 2015; published 17 Jul 2015

Hence, the signals in reflection are less suitable to determine the finesse of the resonator. In the second case, an additional pair of zeroes appears in the in-phase signal. We can show that these secondary zeroes require $r_2^2 \geq (1+3R)/(3+R)$. The solutions then become:

$$f_{\pm} = \pm\frac{f_{\rm FSR}}{\pi}\sin^{-1}\left(\frac{\pi}{2\mathscr{F}}\sqrt{\frac{R(Rr_2^2+3r_2^2-3R-1)}{(1-R)(R^2+r_2^2)}}\right)$$
$$\rightarrow \pm\frac{f_{\rm FSR}}{\pi}\sin^{-1}\left(\frac{\pi}{2\mathscr{F}}\sqrt{\frac{2r_1}{1+r_1^2}}\right) \qquad \text{for } r_2 \rightarrow 1$$

The derivative at the zero crossing of the quadrature phase signal is:

$$\left.\frac{dS_{\rm refl}}{d\phi_f}\right|_{\phi_f=0} = -p_0\, g_{\rm refl}^2\,\frac{R\left(1-r_2^2\right)}{(1-R)^2} = -\left.\frac{dS_{tr}}{d\phi_f}\right|_{\phi_f=0}$$

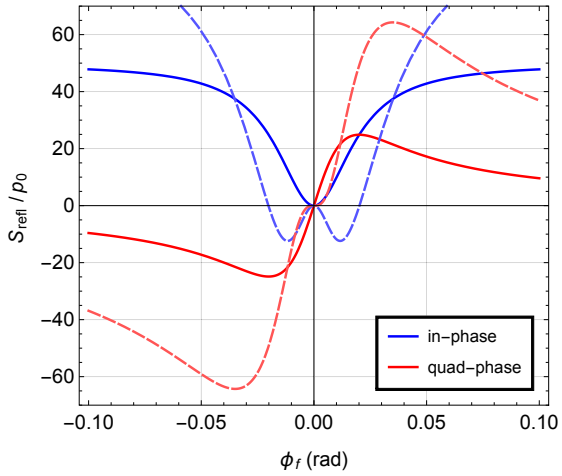

Fig. 5. Double demodulation signal in reflection of a cavity. Shown are the RF in-phase and quadrature-phase signals assuming the audio modulation frequency is small compared to the cavity linewidth. The solid curve represent a cavity with equal transmission front and rear mirrors, whereas the dashed lines represent a cavity with a high reflector as the rear mirror. In both cases the finesse is $\mathscr{F} = 156$.

Acknowledgments

LIGO was constructed by the California Institute of Technology and Massachusetts Institute of Technology with funding from the National Science Foundation, and operates under cooperative agreement PHY-0757058. Advanced LIGO was built under award PHY-0823459. AS would like to thank Columbia University in the City of New York for its support. M. R. acknowledges partial support from NSF-HRD 1242090 and DoD W911NF-13-1-0140. This paper has been assigned LIGO Document No. LIGO-P1400184.

#241606 Received 26 May 2015; revised 2 Jul 2015; accepted 7 Jul 2015; published 17 Jul 2015